



Published in final edited form as:

Anal Bioanal Chem. 2010 July 23; 398(2): 759–768. doi:10.1007/s00216-010-3990-3.

FRET detection of Octamer-4 on a protein nanoarray made by size-dependent self-assembly

Phat L. Tran,

Biomedical Engineering Graduate Interdisciplinary Program, The University of Arizona, Tucson, AZ 85721-0038, USA

Jessica R. Gamboa,

Department of Agricultural and Biosystems Engineering, The University of Arizona, Tucson, AZ 85721-0038, USA, URL: <http://biosensors.abe.arizona.edu>

David J. You, and

Department of Agricultural and Biosystems Engineering, The University of Arizona, Tucson, AZ 85721-0038, USA, URL: <http://biosensors.abe.arizona.edu>

Jeong-Yeol Yoon

Biomedical Engineering Graduate Interdisciplinary Program, The University of Arizona, Tucson, AZ 85721-0038, USA

Department of Agricultural and Biosystems Engineering, The University of Arizona, Tucson, AZ 85721-0038, USA, jyoon@email.arizona.edu, URL: <http://biosensors.abe.arizona.edu>

Abstract

An alternative approach for fabricating a protein array at nanoscale is suggested with a capability of characterization and/or localization of multiple components on a nanoarray. Fluorescent micro- and nanobeads each conjugated with different antibodies are assembled by size-dependent self-assembly (SDSA) onto nanometer wells that were created on a polymethyl methacrylate (PMMA) substrate by electron beam lithography (EBL). Antibody-conjugated beads of different diameters are added serially and electrostatically attached to corresponding wells through electrostatic attraction between the charged beads (confirmed by zeta potential analysis) and exposed p-doped silicon substrate underneath the PMMA layer. This SDSA method is enhanced by vibrated-wire-guide manipulation of droplets on the PMMA surface containing nanometer wells. Saturation rates of antibody-conjugated beads to the nanometer patterns are up to 97% under one component and 58–70% under two components nanoarrays. High-density arrays (up to 40,000 wells) could be fabricated, which can also be multi-component. Target detection utilizes fluorescence resonance energy transfer (FRET) from fluorescent beads to fluorescent-tagged secondary antibodies to Octamer-4 (Oct4), which eliminates the need for multiple steps of rinsing. The 100 nm green beads are covalently conjugated with anti-Oct4 to capture Oct4 peptides (39 kDa); where the secondary anti-Oct4 and F(ab)₂ fragment of anti-gIgG tagged with phycoerythrin are then added to function as an indicator of Oct4 detection. FRET signals are detected through confocal microscopes, and further confirmed by Fluorolog3 spectrofluorometer. The success rates of

© Springer-Verlag 2010

Correspondence to: Jeong-Yeol Yoon.

Preliminary results of this paper were presented at SPIE Defense, Security and Sensing Symposium at Orlando, Florida, USA, 13–17 March 2009, conference number 7313, paper number 731306, and at IEEE/ICME International Conference on Complex Medical Engineering, Tempe, Arizona, USA, 9–11 April 2009.

Electronic supplementary material The online version of this article (doi:10.1007/s00216-010-3990-3) contains supplementary material, which is available to authorized users.

detecting Oct4 are 32% and 14% of the beads in right place under one and two component nanoarrays, respectively. Ratiometric FRET is used to quantify the amount of Oct4 peptides per each bead, which is estimated about 2 molecules per bead.

Keywords

E-beam lithography; Nanometer pattern generation system; Fluorescence resonance energy transfer (FRET); Wire-guide droplet manipulation

Introduction

DNA microarray technologies have successfully been implemented in identifying specific genomic information from living organisms and have become routine practice these days. As microarray analysis is currently being applied to disease state monitoring, drug screening processes, proteomics and cell research, and clinical diagnosis [1-3], more emphasis is given to protein nanoarray technologies. The ability to develop protein nanoarray with well-defined feature size, shape, and spatial configuration is crucial in enhancing signal-to-noise ratio such that signal can be identified individually. The latest techniques and approaches to the fabrication of protein nanoarrays at defined positions and spacing have involved: ink-jet and pipette deposition [4], dip-pen nanolithography (DPN) [5], electron beam lithography [6], and nanocontact printing [7]. However, developing nanoarrays of multiple biomolecules and the ability to retain their full structure and function are still obstacles to be overcome. Proteins are relatively unstable when immobilized on a surface of an array than proteins that are dissolved in buffer. This difficulty is usually seen under sandwich immunoassay, where multiple steps of rinsing are involved such that protein's structure and functionality is altered; thus reducing the ability to detect targets of interest. Therefore, an in situ detection method with limiting rinsing steps is highly warranted. Solving such obstacles will benefit the understanding of biomolecular interactions and dramatically increase the detection limit, preferably at the level of a single molecule.

While DNA sequencing studies provide a better understanding of the genome architecture and gene regulation, protein arrays provide a comprehensive knowledge of genes at a functional level. Proteins are involved in a wide range of biological functions such as catalyzing reactions in living organisms, translating information in cells, regulating biochemical activities, amplifying chemical products, providing mechanical supports, and most importantly, mediating biological defense mechanism [8]. The occurrence of diseases and various cancers take place at the proteomic level, where the expression and distribution of proteins are altered [9]. In response to these diseases, proteins commonly known as biomarkers are secreted at extremely low levels, especially at the early on-set of disease development. This is a serious problem because protein cannot be amplified like DNA. Therefore, methods with extreme sensitivity and high specificity are highly desired for clinical diagnosis and therapeutic applications.

Early detection of protein biomarkers is not only sought after for untreatable diseases or cancers detection but also for stem cell research. Transcriptional proteins involved in differentiating stem cells, like Octamer-4 (Oct4), are present at extremely low volume and in the early stage of cell development [10]. A protein array at nanoscale, which requires much less sample volume and potentially offers single molecular detection of important targets, is expected to play an important role in studying stem cells [11]. The rationale is that controlling the fate of cell differentiation would be critical to stem cell research and offer the possibility of curing untreatable diseases. Unfortunately, the development of protein

nanoarrays and methods for detecting targets at the single-molecule level are still in their infancy.

Among the advances in nanopatterning (as mentioned above), DPN, which uses atomic force microscope equipment to deposit localized add-on materials with the cantilevers on a substrate, is considered as a potential tool for patterning biomolecules on the nanoscale. However, only a limited number of types of proteins, typically two or three, have been patterned in nanometer scale [5]. Furthermore, high-density nanoarrays can also contribute to the success rate of studying proteins or detecting important targets. Recently a 55,000-pen array has been demonstrated for patterning large areas with 80 million dots [12]. However, efforts in multiple-component patterning showed significant complexity in both equipment modification and the process.

Besides the fabrication of a protein nanoarray, a method for single-molecule biorecognition is also warranted. Until now, targets can be detected through electrical properties or optical modalities. While electrical detection may warrant recognition of a single molecule, its ability to study molecular interactions or structural integrities of a protein is limited. On the contrary, Kang et al. have demonstrated the use of dual-color total internal reflection fluorescence microscopy for detection of single molecules of DNA hybridization [13]. However, this deals with DNA not protein, but the concept may be geared toward proteomic study. Furthermore, Huang and Chen have recently illustrated the detection of single molecule by incorporating electrical properties with fluorescence detection. They have applied an electrical potential onto nanowires that were grafted with aptamers to modulate the fluorescence of fluorophores on the target complex [14]. The technique is novel but lacks the ability to study conformational dynamics and interactions of proteins. Thus, characterization, visualization, and detection of important proteins or their dynamic interactions constitute a critical step in biorecognition applications and studying of cell mechanisms.

We have previously reported the assembly of particles on electron beam lithographic patterns [15,16]. In this study, we provide a new approach to the fabrication of protein nanoarrays which involves the vibrated-wire-guide droplet manipulation system, electron beam lithography (EBL) and size-dependent self-assembly (SDSA) of protein-conjugated beads, and fluorescence resonance energy transfer (FRET) to detect Oct4 transcriptional factor. The concept of SDSA is that the larger beads cannot sit in smaller wells while they occupy the larger wells, and smaller beads later fill in the smaller wells to generate a multi-component protein nanoarray. This method allows control of the location of each type of bead and thus control of the location of multiple proteins. For clarity, a schematic representation of the fabrication process is shown in Fig. 1. Ultimately, this new concept of protein nanoarray has the potential to deliver efficient, near real-time, highly sensitive and selective analyses of transcriptional proteins in an effort to control stem cell lineages.

Experimental procedure

Substrate preparation and spin coating

A p-doped silicon wafer (p-type boron, 450–648- μm thick and 4–75- $\Omega\text{-cm}^{-1}$, Exsil, Inc., Prescott, AZ, USA), containing a positive surface charge, was cut into 1 cm^2 chips. Each chip was washed with acetone (Sigma-Aldrich, St. Louis, MO, USA) and isopropyl alcohol (IPA; Honeywell, Chandler, AZ, USA) and subsequently spin-coated with a photoresist, which was made by a 1:1 and 2:3 dilutions of 950 PMMA [poly(methyl methacrylate); Microchem, Newton, MA, USA] with C4 thinner (Microchem), resulting in about 100 and 80 nm layers of PMMA (measured by a profilometer), respectively. The resist was applied to the chip at 500 rpm for 5 s followed by 4000 rpm for 40 s. The chip was then placed on a

hot plate at 180 °C for 1 min to remove any excess residues and to facilitate resist adhesion. The chip was then cooled to room temperature before e-beam patterning.

E-beam lithography and resist development

A FEI Inspec S scanning electron microscope (SEM; FEI Company, Hillsboro, OR, USA) equipped with JC Naby nanometer pattern generation system (JC Naby, Bozeman, MT, USA) was used to etch patterns into the PMMA. Desirable patterns were obtained by the DesignCAD software. The pattern was etched with high voltage of 30 keV at about 10 pA with varying spot size from 1.5 to 3. Each line of pattern was separated by 1 μm and each well was separated by 1 μm center to center considering the limitation of the fluorescence and confocal microscopes' resolution.

After patterning, the etched array was developed with 1:3 methyl isobutyl ketone/isopropyl alcohol (MIBK/IPA; Microchem) developer for 60 s, then 30 s with IPA (Honeywell). Finally, the etched array was washed with deionized water and dried with nitrogen gas.

Covalent attachment of antibodies

Carboxylated, fluorescent polystyrene beads were covalently conjugated with antibodies of interest. The 180 nm glacial blue beads (excitation=380 nm, emission=425 nm, parking area=17.5 \AA^2 per carboxyl group; catalog number FC02F from Bangs Laboratories, Fishers, IN, USA) were covalently conjugated with mouse immunoglobulin G (mIgG; catalog number I5381; Sigma-Aldrich, St. Louis, MO, USA; molecular weight=150 kDa). The 100-nm green beads (excitation=458 nm, emission=510 nm, carboxylated but unavailable parking area; catalog number F8803 from Molecular Probes, Eugene, OR, USA) were covalently conjugated with anti-Oct4 (goat polyclonal antibody; catalog number ab52014; Abcam, Cambridge, MA, USA; molecular weight=150 kDa). The full protocol of covalent antibody conjugation can be found from Bangs Laboratories or Molecular Probes. Basically, different sizes of beads were resuspended in 50 mM 2-(*N*-morpholino)ethanesulfonic acid (Sigma-Aldrich, St. Louis, MO, USA) buffer at pH 6.0 and linked with carbodiimide at room temperature for 15 min. The mixture was centrifuged at 14,000 rpm for 15 min then decanted supernatant and resuspended in 50 mM phosphate-buffered saline (PBS; Sigma-Aldrich, St. Louis, MO, USA) at pH 7.4. Mouse IgG or anti-Oct4 was then covalently conjugated to the 180 nm glacial blue or 100 nm green beads, respectively and slowly rocked overnight at 4 °C to facilitate proper orientation of antibodies. The solution was washed with PBS-BN (10 mM PBS at pH 7.4, 1% BSA and 0.05% sodium azide) and rotated with 40 mM hydroxylamine for 30 min at room temperature to assist in packaging antibodies. Finally, conjugated particles were washed and stored in PBS-BN. The surface coverage of antibodies on the beads were set to 10%.

Development of a protein nanoarray

A 0.5- μl of about 0.025% (*w/v*) solid content of non-antibody-conjugated and antibody-conjugated beads in PBS-BN were serially pipetted onto the protein chip by pipette tips. These droplets of bead suspension were transported to the array area (where the nanometer wells were patterned) using a vibrated metal wire (o.d.=0.5 mm; Fig. 2).

The metal wire was connected to a microcontroller (Arduino Duemilanove, SparkFun Electronics, Boulder, Colorado) interfaced with a USB port that can be programmed to control the three-axis of the droplet manipulator. A Nintendo game pad was attached to the microcontroller so that *x*-, *y*- and *z*-movements of a metal wire could be made possible from the experimenter's input. Details can be found elsewhere [17]. The water contact angle of PMMA is ca. 70°. This is not enough to make "wire-guide" droplet manipulations [17]. Hence, the metal wire was vibrated to make necessary *x*- and *y*- movements. This vibration

provided sufficient energy for micro- and nanobeads to assemble into nanometer wells. Droplets traveled across the patterned area up to three times, followed by removal from that area. Additional droplet of 10 mM PBS was transported and moved over the same area to remove weakly bound particulates. Figure 2 shows the snapshots of these droplet movements, and Fig. 3 shows the experimental setup of a three-axis droplet manipulator. A complete movie is available for this “wire-guide” droplet manipulator system as an Electronic Supplementary Material.

FRET detection

Target biomolecules are Oct4 peptide (catalog number ab20650; Abcam; molecular weight=39 kDa) and anti-mIgG-fluorescein isothiocyanate (anti-mIgG-FITC; catalog number F9006; Sigma; molecular weight=150 kDa). As yellow-dye-conjugated Oct4 is not available, sandwich immunoassay is attempted using yellow-dye-conjugated secondary antibodies. For the detection of Oct4 peptide, 0.5 μ l each of 0.5 mg/ml of secondary anti-Oct4 and donkey polyclonal anti-goat IgG F(ab)₂ fragment tagged with phycoerythrin (anti-gIgG-PE; catalog number 7004; Abcam; molecular weight = 100 kDa for F(ab)₂ and 240 kDa for PE) were applied over the array for about 3 min, which contains 180 nm blue, mIgG-conjugated beads and/or 100 nm green, anti-Oct4-conjugated beads. PE is excited with green color (510 nm) and emits yellow (575 nm). The sequence of fluorescent energy transfer is: blue light source→green beads→yellow PE that is captured by the target. The chip was then rinsed with cold PBS buffer pH 7.4 and mounted in VectaShield mounting medium (catalog number H-1000; Vector Laboratories, Burlingame, CA, USA). The FRET signal is detected by using the spectral analysis available from the C1 Si Laser Scanning Confocal Fluorescence Microscope system. Intensity signals, recorded before and after the presence of targets, were then compared and analyzed using MATLAB (The MathWorks, Inc., Natick, MA, USA). To confirm FRET from the above systems, Fluorolog3 spectrofluorometer (HORIBA Jobin Yvon Inc., Edison New Jersey, NJ, USA) was used at an increment and integration time of 1 s and bandpass of 1 nm for excitation and 1.5 nm for emission. Anti-mIgG-FITC was also used as a negative control, where the sequence of fluorescent energy transfer is: UV light source→blue beads→green FITC in target. (FITC is excited with blue color and emits green, 510 nm). Intensity signals were analyzed in the same manner described above (using MATLAB).

SEM and AFM imaging

The Veeco Dimension 3100 atomic force microscope (AFM) was used to check the etched patterns. It was operated in tapping mode with integral gain of about 0.2 and amplitude of about 1.2 V. The SEM used for e-beam lithography (FEI Inspec S SEM) was also used to image the protein nanoarrays. Due to the sensitivity of PMMA to the electron beam, the Si chips needed to be sputter-coated with gold approximately 5–8 nm thick. The metal coating allowed the sample to be more conductive and provided a protective layer that allowed longer viewing time as well as enhanced signaling of the samples before the PMMA deteriorated.

Results and discussion

Characterization of protein nanoarrays made with size-dependent self assembly

Many fabrication techniques aim at reducing the protein array size, sample volume, or multi-component assay format [1,5-7,12,18,19]. Figures 4 and 5 illustrate the great potential for the development of a protein nanoarray that is capable of improving array scale and density for molecular sensitivity, high-throughput, and quantitative capability. Here, we apply EBL to etch wells on PMMA substrate with thickness of about 80 nm. PMMA thickness is closely related to well size; thinner layers correspond to a reduced aspect ratio and a reduced

minimum feature size. This allows us to pattern well sizes of 80 nm or less depending on the thickness of the polymer. The AFM image in Fig. 4a shows four different wells generated from the EBL for the deposition of antibody-conjugated particles. Each well is separated by approximately 1 μm in x - and y -directions (center-to-center). The size approximated by sectional analysis ranges from 200 nm down to 100 nm. This figure is intended to illustrate that EBL can generate multiple well size such that multi-component protein nanoarray can be generated. The pattern and spatial distribution of those wells can be altered at the desire of the user. This change in design is evidenced in Figs. 4b–c and 5a–c, where each well is separated by 1 μm in x – y direction. Since the detection limit of the fluorescent microscopes is relatively close to the wavelengths in the ultraviolet spectrum, it makes perfect sense to employ the 1 μm separation (center-to-center) between each well. Fortunately, we find that this strategy works better in term of saturation and subsequently detection of targets of interest.

It has been shown that high-density protein arrays can be generated by microcontact printing (soft lithography) and nanocontact printing (DPN) for the possibility of increasing the success rate of detecting targets [12,20]. Here, we attempt to illustrate that EBL in combination with vibrated-wire-guide droplet manipulation system can also achieve a high-density array. The droplet system has allowed us to completely eliminate any washing steps since it has the ability to drag the sample out of the array. The entire array of $200 \times 200 \mu\text{m}$ with each well separated by 1 μm (yielding 40,000 wells) is incorporated with 100 nm carboxylated fluorescent beads by the vibrated-wire-guide droplet manipulator. A 0.5- μl droplet is passed over the array multiple times to improve the saturation rate. Three times of such movements was found to be optimum. The additional energy generated by the vibrated wire and the electrostatic attraction between the carboxylated beads (negatively charged) and p-doped silicon wafer (positively charged) enhance the saturation of beads up to 97% in a nanoarray (Fig. 4b). Although the beads are passivated with proteins, they still carry enough negative charge (zeta potentials of anti-Oct4-conjugated beads are -14.6 ± 0.5 mV for 5% surface antibody coverage and -10.5 ± 0.5 mV for 10% surface antibody coverage, while that of bare beads is -23.5 mV) for electrostatic binding to take place. The 100-nm beads can be seen from nearly all patterned wells under incomplete coating of gold; indicating very high saturation rate and great improvement from our previous work [16].

If a 1-cm^2 array was created, 1 billion wells could be created that can accommodate antibody-conjugated beads. However, this scenario is unlikely to take place because the success rate of depositing antibody-conjugated beads is rather low. In Fig. 4c, which is only a small portion of the entire array, only 47% out of 1,224 possible wells are occupied with antibody-conjugated beads. The average saturation rate from three different experiments is $39 \pm 8\%$. This low rate of saturation is very likely to be due to the fact that the 0.5 μl droplet is passed over the array only once. Passing the antibody-conjugated beads over the array multiple times will certainly increase the saturation rates but also risk non-specific attachment of antibody-conjugated beads, as proteins have a tendency to adsorb on many plastic surfaces in aqueous media if sufficient contact time is provided. We actually attempted to pass a droplet of antibody-conjugated beads three times (same as plain beads), but found many beads outside of wells. However, this non-specific attachment may not be a problem, as each position on the wells can easily be identified under the microscope (separated by 1 μm) so that we can ignore any signals coming from the outside of the wells.

Our work in single-component nanoarray has allowed us to fabricate nanoarray of multiple components based on the size of the beads. The rationale is that once the larger beads occupy the larger wells, but cannot sit in smaller wells, smaller beads can occupy the smaller wells such that size-dependent self-assembly protein nanoarray can be generated [16]. Here, the 180-nm beads are deposited first then followed by smaller beads. The concept is

confirmed in Fig. 5a where the SEM image shows the 180 nm bead sits in a well at about 200 nm and the 100 nm beads in a well of about 110 nm. One of the 200-nm wells, not occupied by the proper bead, is incorporated with four smaller beads. Wells are not perfectly circle due to shifting of astigmatism of the SEM. The other SEM image in Fig. 5b illustrates the great potential to generate protein nanoarray of the system. The 100-nm beads sit in wells of about 130 nm while the 80-nm beads sit in 100-nm wells. However, there are instances where 80-nm beads occupied larger wells that intended for 100-nm beads. There are also cases where multiple beads agglutinated at the same well. However, SDSA is a still plausible concept for the fabrication of multi-component nanoarray. The success rate of incorporating the right beads into the right well's size is relatively high. Figure 5c illustrates that the saturation rate of blue beads (180 nm) in the proper wells is 58% of wells whereas the success rate of proper incorporation of green beads (100 nm) is 70% of wells, as shown in Fig. 5c. (Fig. 5c is a representative result out of three different experiments; the overall average saturation rates of beads are $59\pm 2\%$ for blue and $65\pm 9\%$ for green.) All beads are antibody-conjugated. Furthermore, 30% of green beads (100 nm) are found in the wrong wells while only 2% of the blue beads (180 nm) are in the smaller wells. This pattern suggests that unoccupied wells are more likely to be inhabited by smaller beads. This problem may become worse for the smallest beads in three- or four-component system. One solution to overcome this problem is optimization of the protocol with vibrated-wire-guide manipulation. In the practical situation with confocal/fluorescent microscopy, however, the location and spatial distribution of conjugated beads can easily be identified as each bead has a distinctive emission, such that the wrong incorporation of conjugated beads can be disregarded in data analysis.

FRET detection of Oct4

While proteomic approaches such as circular dichroism (CD) spectroscopy have been deployed to study the secondary structure of proteins [21], protein arrays on the other hand provide better detection of protein expression or the presence of a biomarker at varying levels. Here, we are utilizing a fluorescence based method (FRET) in conjunction with optical detection (confocal microscopy and spectrofluorometry) for the potential of single-molecule level detection and possible investigation of molecular interactions on a protein array format. For FRET to take place in our scheme, the acceptor (target protein or its secondary antibody) must be within close proximity (1–10 nm) of the donor (fluorescent beads). Also, the absorption spectrum of the acceptor must overlap fluorescence emission spectrum of the donor [22]. Since the size of antibodies is about 8 nm [23-25], and considering the possible orientation for protein attachment and target captures in Figs. 4d and 6 (insets), FRET is very likely to take place. Another advantage of using FRET is its ability to minimize false-positive signals originating from multiple steps of rinsing. Targets have to be captured or bound closely to elicit FRET.

Figure 4c–d establishes the detection of Oct4 through FRET on a single-component nanoarray format. Both images are collected and analyzed by using the spectral analysis under the C1 Si laser scanning confocal fluorescence microscope. Here, the emission from 100 nm carboxylated, green fluorescent beads (donor) that excite at 458 nm excites the fluorophore phycoerythrin (acceptor) that is attached to Oct4 via secondary antibodies; thus emitting more fluorescent signals at about 575 nm (Fig. 4d inset). Figure 4c is captured from the confocal microscope using spectral mode, showing single beads at which some contain FRET signals and some do not. Three specific spots are selected to illustrate raw spectrums at the resolution of 5 nm from 32 channels, showing the emission intensity against wavelength. The first box (red) represents the background signal. This signal is very likely to be coming from the autofluorescence of the PMMA polymer. The second box (aqua) represents fluorescent signals emitted by the 100 nm beads. The third box (purple) illustrates

FRET signals from the 100 nm beads, where the spot is highly fluorescing with higher emission intensity at about 575 nm, indicating the presence of Oct4. To confirm this, the ratio of intensity (ROI) is evaluated by dividing the maximum intensity of the acceptor emission (575 nm) by the maximum intensity of the donor emission (510 nm; ratiometric FRET) [26-28]. ROI of one hundred spots are collected and subsequently corrected with background signals to extract the actual emission intensity from the beads and their target indicators. A histogram of that 100 spots is postulated to discern which spot is most like to exhibit FRET. Hence, a general result is summarized in Fig. 4d, where the average ROI of spots with FRET is being significantly higher than that without FRET ($p < 0.05$). These results establish the basis of FRET as a plausible principle for targets detections under nanoarray format.

Assuming that the highly fluoresced spots are potential FRET, Fig. 4c has about 32% of the 47% saturation of antibody-conjugated 100 nm beads illustrating the capturing of Oct4 (on average, $33 \pm 1\%$ of the beads in right place exhibit FRET). Our system is able to separate each individual antibody-conjugated bead in order to enhance and increase the chance of capturing an individual molecule or target. For instance, the surface area of a 100-nm bead ($31,416 \text{ nm}^2$) can be completely saturated with 465 IgGs if the surface area of the IgG is 67.5 nm^2 [26]. However, only about a quarter of antibodies on the bead will be exposed and oriented correctly under a perfect scenario. If such a case exists, a 100-nm bead can perfectly express about 116 IgGs for any given purpose. This calculation also reveals that a 10 nm bead can express about one IgG, which can ideally demonstrate true single-molecule detection. Unfortunately, etching a well that would isolate a single 10-nm bead is considered very difficult with current e-beam lithographic technology. Additionally, the thickness of PMMA layer should be made equivalent to the wells' diameter (10 nm), which cannot serve as an isolation barrier between the electrostatic forces. In this work, therefore, we set the surface coverage of antibodies not at its saturation but to 10%, resulting about 12 IgGs per each bead, which may lead to near-single-molecule-level detection.

The detection of Oct4 through FRET is also persistent with two component nanoarray (Fig. 5c-d). Here, 180-nm blue beads conjugated with mIgG and 100 nm green beads conjugated with anti-Oct4 are deposited accordingly to generate the protein nanoarray. Samples containing Oct4 peptide, anti-Oct4, anti-gIgG-PE are then added over the array as described above. The spectral image is then collected and processed by using the confocal microscope. The Fig. 5c is digitally zoomed in to illustrate blue and green beads in alternating patterns.

In terms of Oct4 detection, 100 green spots are selected to calculate for the ROI at 575 nm over 510 nm. Similar to Fig. 4c, three different spots are selected to illustrate the raw emission intensity spectrum (Fig. 5d). The red box corresponds to the red graph in Fig. 5d, representing the background signal. The aqua box represents the green beads without target or FRET. The purple box represents the spot with possible FRET. It is also evidenced that the emission intensity at 575 nm of a FRET spots is much higher than the spot without FRET. Therefore, spots with FRET should have a higher ROI comparing to spots without FRET. After correcting the background noise, a histogram is generated to locate which spots with 95% or higher confidence in exhibiting FRET. Hence, 19% of the 100 nm green beads in right place exhibit the detection of Oct4 ($p < 0.05$), where the ROI is 0.291 ± 0.03 (Fig. 5d; again, Fig. 5c and d is a representative result out of three different experiments; the average fraction of beads that exhibit FRET is $18 \pm 1\%$). The inset in Fig. 5d is a linear relationship between the concentration of anti-gIgG-PE and the ratio of maximum intensity at about 575 nm (acceptor emission) over 510 nm (donor emission). It shows that a ROI of about 0.291 is correlated to a concentration of about $5 \mu\text{g/ml}$. As the molecular weight of anti-gIgG-PE is $340 \text{ kDa} = 340 \text{ kg/mol}$, the corresponding molar concentration is 1.5 nM . Assuming that the target Oct4, anti-Oct4, and anti-gIgG-PE bind to each other at the ratio of 1:1:1 (for rough

estimation), the concentration of the target Oct4 can also be approximated as 1.5 nM. As the beads/wells are separated by 1 μm , we can also assume that the target Oct4 within a hemisphere of 1 μm radius can be attracted to the beads during vibrated droplet movements. Multiplying the concentration 1.5 nM (=1.5 nmol/l) by the volume of the hemisphere [= $(4/3) \times \pi \times (1 \mu\text{m})^3 / 2 = 2.1 \mu\text{m}^3$] gives 3.1×10^{-24} mol. Multiplying this number by Avogadro's number 6.02×10^{23} /mol gives 1.9 molecules, potentially indicating single-molecule level detection. This number is not far off from the number of IgGs per each bead that is calculated above, about 12.

Meanwhile, we could not find any blue beads that might indicate FRET simply because the donor (blue beads) and the acceptor (anti-IgG-PE) are not a match. Furthermore, we did not encounter any orange fluorescent in on the blue beads. Therefore, FRET can ensure the right detection of targets and eliminate any false-positive signals. Furthermore, it has a potential to investigate the antibody-antigen interactions and functions.

The detection of Oct4 through FRET is further confirmed by using the Fluorolog3 Spectrofluorometer (Fig. 6). According to HORIBA Jobin Yvon Inc., this particular instrument can detect 50 fM fluorescein. Here, 180-nm glacial blue beads are conjugated with mIgG, where anti-mIgG-FITC is added as a target indicator. On the other hand, 100 nm green beads are conjugated with anti-Oct4 to capture Oct4 peptide where the secondary anti-Oct4 and anti-IgG-PE acts as an indicator to the detection of Oct4. Graphs A and B of Fig. 6 demonstrate FRET at 520 nm for anti-mIgG-FITC and 575 nm for Oct4 peptide. The emission intensity recorded from each solution is normalized to 1 and extrapolated based on the controls to illustrate FRET and to calculate the area under the curve. The ratio between area under normal and FRET curves is relative to the energy transmission efficiency. For 180-nm blue beads, a 15.24% transmission is found but only 14.46% for the 100-nm green beads. This is rather comprehensible because of the distance from the acceptor (anti-IgG-PE, anti-Oct4, Oct4 peptide) and to the donor (beads); thus yielding a lower energy transmission in detecting Oct4 than anti-mIgG. This rationale is further confirmed with 50-nm green beads, where the energy transmission is found to be 13% (results not shown). Considering the size of IgG [29] along with the required distance and energy-transfer efficiency for FRET [30], the FRET efficiency found here is relatively within the realm of possibility.

Conclusions

The developments reported in this paper combine the vibrated-wire-guide droplet manipulation system, e-beam lithography, and size-dependent self-assembly of antibody-conjugated beads to develop a multiple component protein nanoarray. Spectral images collected by the confocal microscopes are an important tool to quantitatively determine the detection of Oct4 through fluorescence resonance energy transfer, without the need for multiple rinsing steps commonly required in a sandwich immunoassay format. Finally, the detection of Oct4 through FRET signal is confirmed by the Fluorolog3 Spectrofluorometer, suggesting that FRET is an efficient biorecognition method to detect important targets and can possibly be used to study molecular interactions under a nanoarray. In perspective, we will also deepen our investigation on the use of this protein nanoarray to manipulate and control cells proliferation and migration, an important ongoing process in tissue engineering.

Supplementary Material

Refer to Web version on PubMed Central for supplementary material.

Acknowledgments

The authors thank Dr. Brooke Beam and Paul Lee of the Keck's facility for their assists in AFM, SEM, and confocal imaging, and Dr. Urs Utzinger and Ronnie George for the use and assistance of Fluorolog3 spectrofluorometer. In addition, authors would like to acknowledge Yee Tchao for her early contribution in this project and Vincent Wong for assistance in measuring zeta potential of beads. This work was supported by U.S. National Institute of Health under grant R03EB006754, as well as fellowship supports for Phat L. Tran (NIH-Initiative for Maximizing Student Diversity Fellowship and NIH-Cardiovascular Training Grant HL007955).

References

1. Nicolan, DV.; Demers, L.; Ginger, DS. Microarray technology and its applications. Springer; New York: 2005.
2. Wingren C, Borrebaeck CAK. Progress in miniaturization of protein arrays—a step closer to high density nanoarrays. *Drug Discov Today*. 2007; 12:813–819. [PubMed: 17933681]
3. MacBeath G. Protein microarrays and proteomics. *Nat Genet*. 2002; 32:526–532. [PubMed: 12454649]
4. Hasnma PK, Drake B, Marti O, Gould SA, Prater CB. The scanning ion-conductance microscope. *Science*. 1989; 243:641–643. [PubMed: 2464851]
5. Lee KB, Lim JH, Mirkin CA. Protein nanostructures formed via direct-write dip-pen nanolithography. *J Am Chem Soc*. 2003; 125:5588–5589. [PubMed: 12733870]
6. Tseng AA, Chen K, Chen CD, Ma KJ. Electron beam lithography in nanoscale fabrication: recent development. *IEEE Trans Electron Packag Manuf*. 2003; 26:141–149.
7. Li HW, Muir BVO, Fichet G, Huck WTS. Nanocontact printing: a route to sub-50 nm-scale chemical and biological patterning. *Langmuir*. 2003; 19:1963–1965.
8. Petsko, GA.; Ringe, D. Protein structure and function. New Science; London, UK: 2004.
9. Hanash S. Diseases proteomes. *Nature*. 2008; 422:226–232. [PubMed: 12634796]
10. Niwa H, Toyooka Y, Shimosato D, Strumpf D, Takahashi K, Yagi R, Rossant J. Interaction between Oct3/4 and Cdx2 determines trophectoderm differentiation. *Cell*. 2005; 123:917–929. [PubMed: 16325584]
11. Vega RA, Maspocho D, Salaita K, Mirkin CA. Nanoarrays of single virus particles. *Angew Chem Int Ed*. 2005; 44:6013–6015.
12. Salaita K, Wang Y, Fragala J, Vega RA, Liu C, Mirkin CA. Massively parallel dip-pen nanolithography with 55,000-pen twodimensional arrays. *Angew Chem Int Ed*. 2006; 45:7220–7223.
13. Kang SH, Kim YJ, Yeung ES. Detection of single-molecule DNA hybridization by using dual-color total internal reflection fluorescence microscopy. *Anal Bioanal Chem*. 2007; 387:2663–2671.
14. Huang S, Chen Y. Ultrasensitive fluorescence detection of single protein molecules manipulated electrically on Au nanowires. *Nano Lett*. 2008; 8:2829–2833. [PubMed: 18666800]
15. Powell T, Yoon JY. Fluorescent biorecognition of gold nanoparticle-IgG conjugates self-assembled on e-beam patterns. *Biotechnol Prog*. 2006; 22:106–110. [PubMed: 16454499]
16. Powell TB, Tran PL, Kim K, Yoon JY. Size-dependent self-assembly of submicron/nano beads-protein conjugates for construction of a protein nanoarray. *Mater Sci Eng C*. 2009; 29:2459–1463.
17. Yoon JY, You DJ. Backscattering particle immunoassays in wire-guide droplet manipulations. *J Biol Eng*. 2008; 2:15. [PubMed: 19014703]
18. Lynch M, Mosher C, Huff J, Nettikadan S, Johnson J, Henderson E. Functional protein nanoarrays for biomarker profiling. *Proteomics*. 2004; 4:1695–1702. [PubMed: 15174138]
19. Ramanujan CS, Sumitomo K, de Planque MRR, Hibino H, Torimitsu K, Ryan JF. Self-assembly of vesicle nanoarrays on Si: a potential route to high density functional protein arrays. *Appl Phys Lett*. 2007; 90:033901.
20. Delehanty JB, Ligler FS. A microarray immunoassay for simultaneous detection of proteins and bacteria. *Anal Chem*. 2002; 74:5681–5687. [PubMed: 12433105]

21. Narra HP, Cordes MHJ, Ochman H. Structural features and the persistence of acquired proteins. *Proteomics*. 2008; 8:4772–4781. [PubMed: 18924109]
22. Ciruela F. Fluorescence-based methods in the study of protein-protein interactions in living cells. *Curr Opin Biotechnol*. 2008; 19:338–343. [PubMed: 18602005]
23. Bacher G, Szymanski WW, Kaufman SL, Zoller P, Blaas D, Allmaier G. Charge-reduced nano electrospray ionization combined with differential mobility analysis of peptides, proteins, glycoproteins, noncovalent protein complexes and viruses. *J Mass Spectrometry*. 2001; 36:1038–1052.
24. Hartman WK, Saptharishi N, Yang XY, Mitra G, Soman G. Characterization and analysis of thermal denaturation of antibodies by size exclusion high-performance liquid chromatography with quadruple detection. *Anal Biochem*. 2004; 325:227–239. [PubMed: 14751257]
25. Leonard FP, Elliot JT, Tsai DH, Zachariah MR, Tarlov MJ. Determination of protein aggregation with differential mobility analysis: application to IgG antibody. *Biotechnol Bioeng*. 2008; 101:1214–1222. [PubMed: 18980182]
26. Tadross MR, Park SA, Veeramani B, Yue DT. Robust approaches to quantitative ratiometric FRET imaging of CFP/YFP fluorophores under confocal microscopy. *J Microsc*. 2009; 233:192–204. [PubMed: 19196425]
27. Ko S, Grant SA. Development of a novel FRET method for detection of *Listeria and Salmonella*. *Sens Actuators, B*. 2003; 96:372–378.
28. Zhang CY, Yeh HC, Kuroki MT, Wang TH. Single-quantum-dot-based DNA nanosensor. *Nat Mater*. 2005; 4:826–831. [PubMed: 16379073]
29. Boehm MK, Woof JM, Kerr MA, Perkins SJ. The Fab and Fc fragments of IgA1 exhibit a different arrangement from that in IgG: a study by X-ray and neutron solution scattering and homology modeling. *J Mol Biol*. 1999; 286(5):1421–1447. [PubMed: 10064707]
30. Hausteine E, Jahnz M, Schwille P. Triple FRET: a tool for studying long-range molecular interactions. *Chem Phys Chem*. 2003; 4:745–748. [PubMed: 12901306]

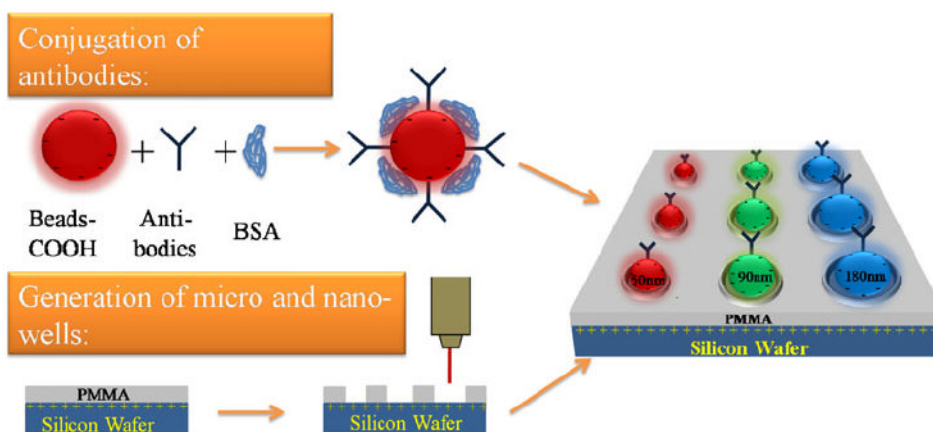


Fig. 1. Schematic illustration of the protein nanoarray fabrication process using electron beam lithography to create micro- and nano-wells, onto which antibody-conjugated beads are self-assembled from the larger to the smaller beads. *Beads-COOH* carboxylated micro- and nanobeads. *BSA* bovine serum albumin (to passivate the beads). Silicon wafer is p-doped with spin-coated layer of polymethyl methacrylate (*PMMA*)

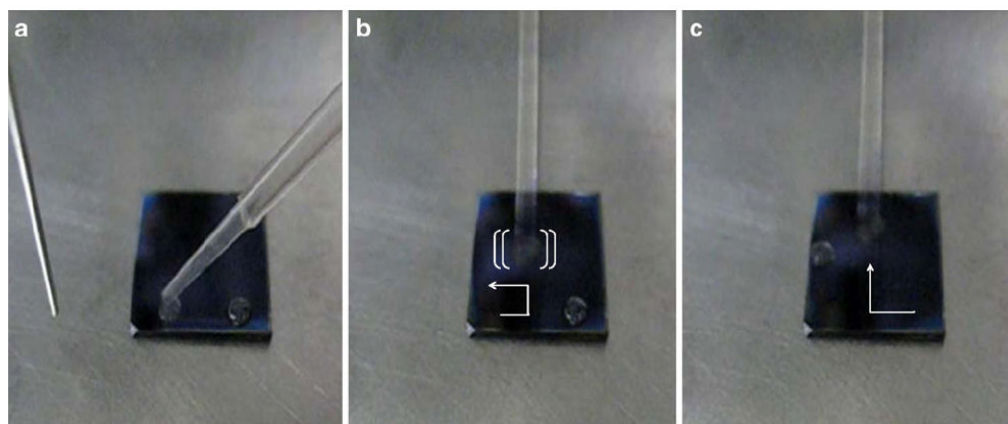


Fig. 2. Snapshots of droplet manipulation for SDSA array. **a** A droplet of beads is suspended and **b** a vibrating metal wire transports the droplet over the array. **c** Another droplet of beads is immobilized over the array

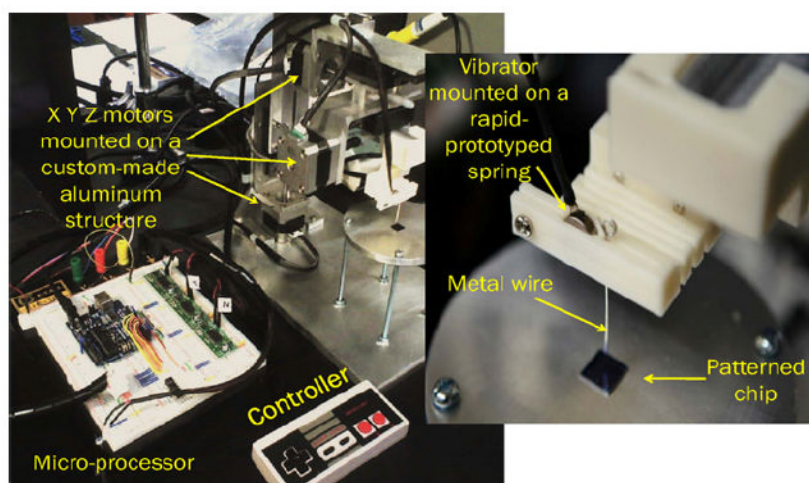


Fig. 3. Experimental setup of three-axis droplet manipulator. The vibrator is mounted on a rapid-prototyped plastic spring such that the metal wire can vibrate to assist in generating high-density arrays

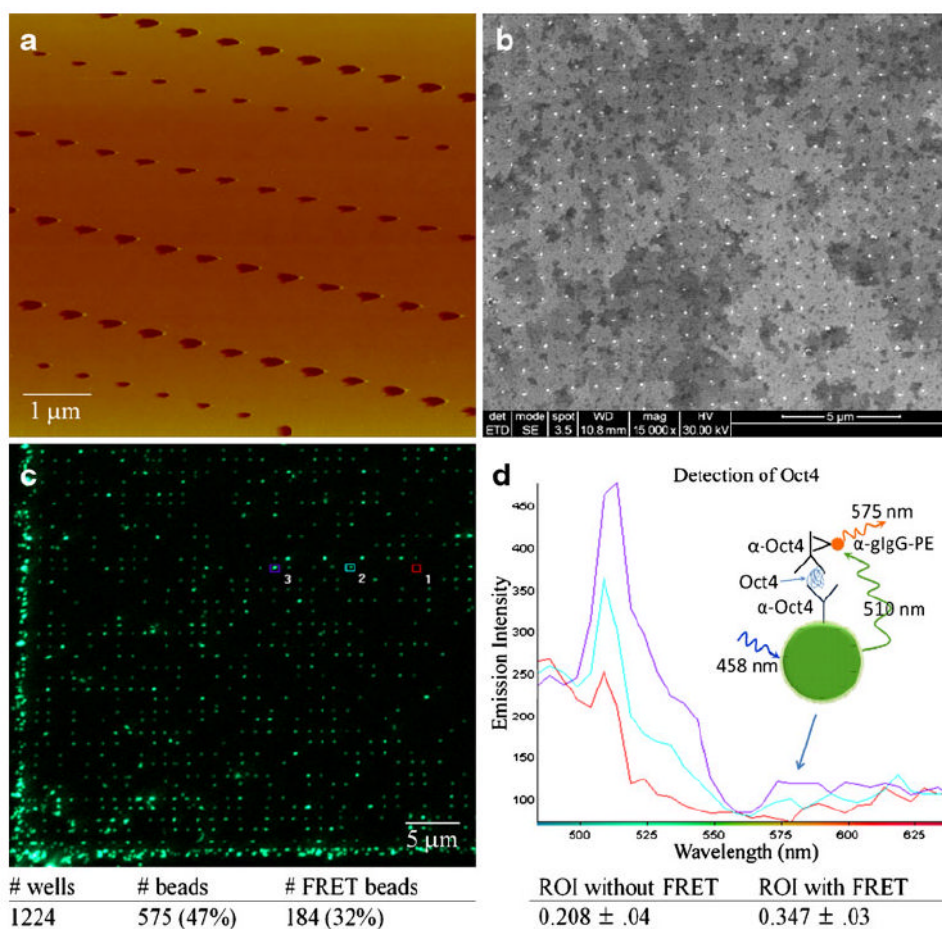


Fig. 4. High-density one-component protein nanoarray. **a** The AFM image of the patterned wells capable of making nanoscale protein array. Each well is separated by 1 μm (center-to-center). The smallest well is about 100 nm (to accommodate 80 nm beads). **b** High-density nanoarray containing 100 nm beads. Each bead is separated by 1 μm (center-to-center). **c** Spectral image of 100-nm green beads. The image is digitally zoomed by the confocal microscope illustrating some FRET signals. The table below the image summarizes the number of beads involved. **d** Raw spectrums collected from three spots in **c**. The table shows that the spots with FRET have higher ratio of intensity (ROI; 575 nm/510 nm) than the spots without FRET ($p < 0.05$). The average ROI is evaluated from all applicable beads, not just three places. The *inset image* demonstrates the possible pathway from exciting the donor to emitting FRET from the acceptor

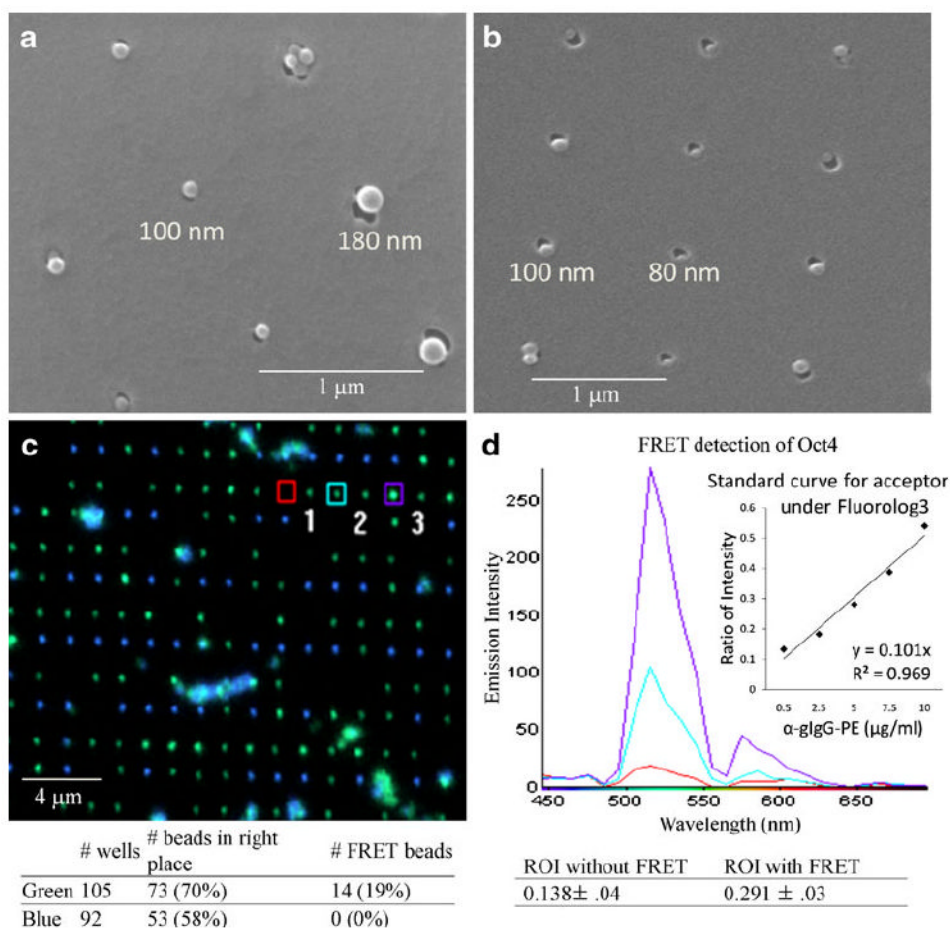


Fig. 5. Multi-component SDSA protein nanoarray for the detection of Oct4. **a** SEM image of 180 and 100 nm beads bound to their corresponding wells size. **b** SEM image of 100 and 80 nm beads nanoarray. **c** Spectral image of 180-nm blue mIgG-conjugated beads and 100-nm green anti-Oct4 conjugated beads. The table below the image summarizes the number of beads involved. **d** Raw spectrums collected from three locations in **c**, illustrating the detection of Oct4 through FRET signals. The *inset* graph shows the linear relationship between the concentration of F(ab)₂ fragment of anti-gIgG-PE and the ROI (575 nm/510 nm). The average ROI is evaluated from all applicable beads, not just three places. This relationship is then correlated with the ROI from each spot on the confocal spectrum image to determine the detection limit

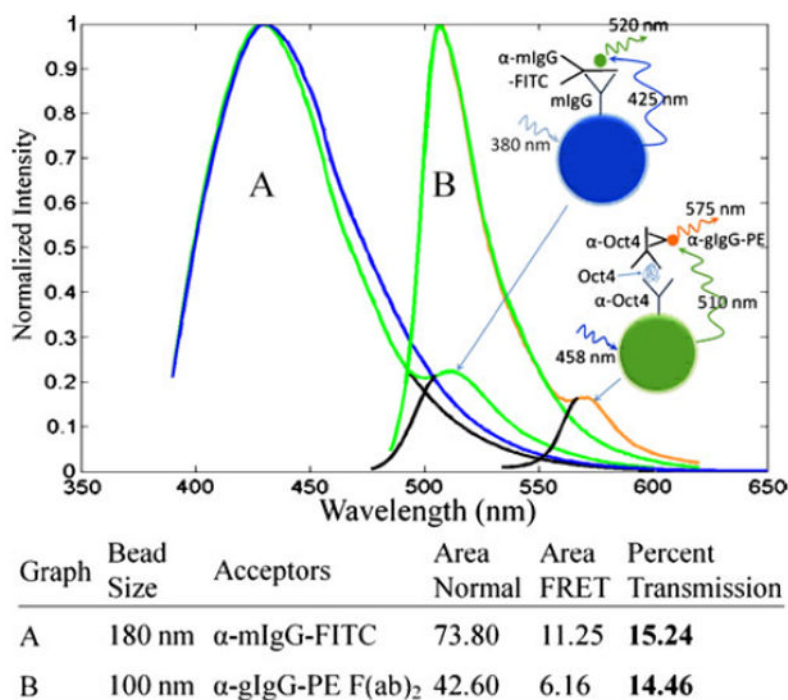


Fig. 6. Detection of Oct4 under Fluorolog3 spectrofluorometer. The intensity signals are normalized to 1 at the maximum point. **a** The blue line represents the emission signal from the 180 nm mIgG-conjugated blue beads spectrum without the target. The green line represents the emission from the beads and the target indicator anti-mIgG tagged with FITC. **b** The green line represents the emission from 100 nm anti-Oct4-conjugated green beads without the target. The orange line represents the emission of the bead and the target indicators, anti-gIgG-PE, anti-Oct4 and Oct4, confirming the detection Oct4 through FRET signals. The table summarizes the area under the curve and transmission of FRET. The insets demonstrate the possible pathway from exciting the donor to emitting FRET from the acceptor